

# Condition assessment of electro-mechanical actuators for aerospace using relative density-ratio estimation

M. Mazzoleni\*, M. Scandella\*, Y. Maccarana\*, F. Previdi\*,  
G. Pispola\*\*, N. Porzi\*\*

\* *Department of Management, Information and Production engineering  
University of Bergamo, via Galvani 2, 24044 Dalmine (BG), Italy  
(e-mail: mirko.mazzoleni@unibg.it).*

\*\* *Umbra Group, 06034 Foligno (PG), Italy*

**Abstract:** This paper faces the problem of developing an effective Condition Monitoring algorithm (CM) for Electro-Mechanical Actuators (EMA) in aerospace applications. In this view, a test campaign has been carried out in order to progressively bring the EMA near to failure, by means of a test bench suitably developed. Various indicators have been computed from measured data, for a set of the EMA's working regimes. The statistical distribution of the computed features is assessed and tracked over time. We propose an online statistical approach, based on density estimation techniques, in order to detect potential changes in the data distribution. The discovered changes are then interpreted as a modification of the EMA's health state, leading to a first building block for a complete condition assessment strategy.

© 2018, IFAC (International Federation of Automatic Control) Hosting by Elsevier Ltd. All rights reserved.

*Keywords:* Condition monitoring; Change-point detection; Kernel methods; Time-series

## 1. INTRODUCTION

The More Electric Aircraft (MEA) initiative aims to increase the employment of electrical systems in aerospace environments, in order to decrease weight and further develop overall efficiency and reliability, Sarlioglu and Morris (2015). Even though the reliability of hydraulic actuators (see Cologni et al. (2016) for a modeling activity on these types of actuators) is known to be high, the oil distribution is bulky and prone to leaks, Buticchi et al. (2017). The importance of this transition has been understood by leading companies in the field such as Boeing and Airbus. Representative examples are models like A380, see Buticchi et al. (2017) and Boeing 777, Boeing 787, see Yeh (1996); Buticchi et al. (2017) respectively. The more electric aircraft mission has been embraced not only by those individual companies, but also on a larger geographical scale: European and American research projects are constantly issued with this purpose in mind. In this setting, fault detection and monitoring of EMAs emerged as important topics to be investigated Garcia et al. (2008). One of the latest researches in this area is the FP7 EU-funded HOLMES project: in Mazzoleni et al. (2017a,c), the authors presented an experimentally-validated model-based and a data-driven method for fault detection of EMAs used in airliner applications. The same issue is faced in the NASA-funded project Balaban et al. (2015), where the authors developed also a prognostic method for a flyable test-bed.

Despite recent advantages in the field, corroborated by continuous private and public investments, the goal of a more electric aircraft is still far away. This does not mean we have to stop investing. It is exactly this principle which

led to the birth of the REPRISE project, Mazzoleni et al. (2017b). The aim of the project is to support the improvement of the Technological Readiness Level (TRL) for a Flight-Control System (FCS) of small aircrafts, bringing it to TRL 5. A critical part of the work needed to reach the goal is the development of a Condition Monitoring (CM) or Health Monitoring (HM) system, able to provide a continuous assessment of the EMA health state, tracking the progressive faults degradation. The present work has been carried out in the context of the REPRISE project. A large endurance test activity has been performed on a real-scale EMA, and experimental data have been measured. The proposed monitoring algorithm leverages on the information acquired from the test bench, in order to assess the progressive degradation.

Monitoring approaches have been previously faced by the aerospace community. In Byington et al. (2004), the author proposes a data-driven prognostic and health monitoring approach on Electro-Hydraulic Servo Valves (EHSV), stating the seamless adaptation of the method to EMAs. A condition monitoring approach suited specifically for EMAs is presented in Dixon and Pike (2002), where, instead, a model-based approach is pursued by tracking the estimates of a model's parameters. A health monitoring strategy based on EMAs' position-tracking performance has been recently proposed by Di Rito et al. (2017). As usually done with mechanical components, authors in Ismail et al. (2016) proposed a fault detection strategy based on vibration analysis.

In contrast with the latter two references, the work presented in this paper relies on an *unsupervised nonparametric data-driven* method, *using only* features computed

from phase-current measurements. The method employed here is a change-detection algorithm based on *density-ratio estimation*, Liu et al. (2013). The rationale of the method consists into assessing if a change occurred between the probability distributions of time-series samples over past and present intervals, as in the seminal work of Basseville et al. (1993). The working hypothesis is that, if a significant change occurred in the data distribution, the monitored system degraded its functionalities.

Change-point detection methods can be classified into two categories: Real-time detection, Garnett et al. (2009), and retrospective detection, Yamanishi and Takeuchi (2002). The former methods give an immediate response, while retrospective techniques permit to have higher detection accuracy for higher computation times. The algorithm employed in this paper belongs to the retrospective category. The choice is dictated by the fact that we prefer to have a more reliable answer for a problem which usually exhibits a slow degradation trend. Therefore, a real-time detection is not necessary. Subspace methods, particularly fond to the system identification community, has gained high popularity in recent years as a mean to perform change-detection, Kawahara et al. (2007). This further motivates the research in similar methods, as the one employed in this work, by researchers in system identification.

The remainder of the paper is organized as follows. Section 2 formulates the change-detection problem. Section 3 presents the experimental setup deployed for the performed endurance tests on the EMA. In Section 4, the density-ratio change detection method is adapted to perform condition monitoring of the EMA under study, discussing also experimental results on data measured from an endurance test campaign. Lastly, Section 5 is devoted to concluding remarks and future developments.

## 2. CHANGE DETECTION VIA RELATIVE DENSITY-RATIO ESTIMATION

### 2.1 Problem statement

In this paper, we employ a density-ratio estimation method known as *Relative unconstrained Least-Squares Importance Fitting* (RuLSIF), see Kanamori et al. (2009); Liu et al. (2013). The algorithm is built assuming that the estimation of the *ratio* of two densities is substantially easier than estimating the two densities in a separate way, Sugiyama et al. (2012). In our setting, the two densities represents kernel estimates of the time series data distribution, before and after a certain time instant. Once these densities (or, as stated, their ratio) have been estimated, it is possible to assess how much they differ, by using suitable divergences, see Gibbs and Su (2002). Density ratio estimation is a useful tool in both machine learning and statistical community. However, due to the unbounded nature of density ratio, the estimation procedure can be vulnerable to corrupted data points, which often pushes the estimated ratio toward infinity. For these reasons, a *bounded* (relative) density-ratio estimator was introduced in Liu et al. (2013), and it will be employed in this work.

Let  $\mathbf{y}(t) \in \mathbb{R}^{d \times 1}$  be a  $d$ -dimensional time-series sample at time  $t$ . Let

$$\mathbf{Y}(t) \equiv [\mathbf{y}(t)^\top, \mathbf{y}(t+1)^\top, \dots, \mathbf{y}(t+k-1)^\top]^\top \in \mathbb{R}^{d \cdot k \times 1}$$

be a “subsequence”<sup>1</sup> of time-series of length  $k$ , at time  $t$ . The subsequence  $\mathbf{Y}(t)$  is treated as a single data sample. We then define the quantity  $\mathcal{Y}(t)$  as the matrix composed by  $n$  of the  $dk$ -th dimensional samples  $\mathbf{Y}(t)$ , starting from  $t$ :

$$\mathcal{Y}(t) \equiv [\mathbf{Y}(t), \mathbf{Y}(t+1), \dots, \mathbf{Y}(t+n-1)] \in \mathbb{R}^{d \cdot k \times n}.$$

The matrix  $\mathcal{Y}(t)$  forms a *Hankel matrix*, playing a key role in change-point detection based on subspace learning, Kawahara et al. (2007). Consider now two consecutive segments  $\mathcal{Y}(t)$  and  $\mathcal{Y}(t+n)$ . The change-detection problem is then solved by computing a certain dissimilarity measure between  $\mathcal{Y}(t)$  and  $\mathcal{Y}(t+n)$ . The higher the dissimilarity measure is, the more likely the two distributions differ. The entire notations are depicted schematically in Figure 1.

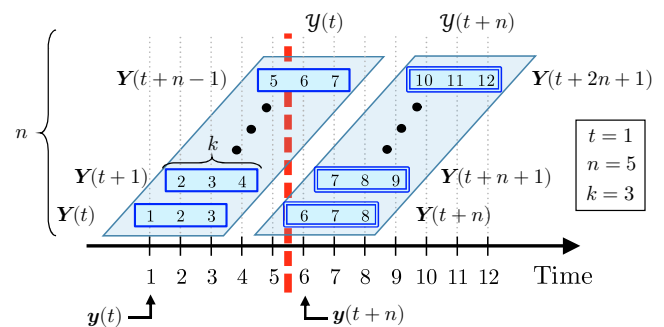


Fig. 1. Schematic representation of the notation for a one-dimensional time series, for illustrative settings such that  $d = 1, t = 1, n = 5$  and  $k = 3$

### 2.2 Divergence measures

Denote now the probability distributions of the samples in  $\mathcal{Y}(t)$  and  $\mathcal{Y}(t+n)$  as  $P$  and  $P'$ , respectively. The Pearson divergence is defined as, Pearson (1992):

$$\text{PE}(P \| P') \equiv \frac{1}{2} \int p'(\mathbf{X}) \cdot \left( \frac{p(\mathbf{X})}{p'(\mathbf{X})} - 1 \right)^2 d\mathbf{X}, \quad (1)$$

where  $\mathbf{X}$  denotes the generic  $dk$ -th dimensional random variable, and  $p(\mathbf{X})$ ,  $p'(\mathbf{X})$  are the probability density functions of  $P$  and  $P'$ , respectively.

Let now  $\{\mathbf{Y}_i\}_{i=1}^n$  and  $\{\mathbf{Y}'_j\}_{j=1}^n$  be a set of samples drawn from  $p(\mathbf{X})$  and  $p'(\mathbf{X})$ . In order to compute (1), we will employ an *estimate* of the density-ratio  $\frac{p(\mathbf{X})}{p'(\mathbf{X})}$ , using proper sets of samples which are representative of the two distributions. The samples  $\{\mathbf{Y}_i\}_{i=1}^n$  are those belonging to  $\mathcal{Y}(t)$ . The samples  $\{\mathbf{Y}'_j\}_{j=1}^n$  are those belonging to  $\mathcal{Y}(t+n)$ .

The density-ratio value  $\frac{p(\mathbf{X})}{p'(\mathbf{X})}$  in (1) could be unbounded, depending on the condition of the denominator density  $p'(\mathbf{X})$ . To overcome this problem, the  $\alpha$ -relative Pearson divergence measure was introduced in Liu et al. (2013), for  $0 \leq \alpha < 1$ , as:

<sup>1</sup> For higher-dimensional time-series,  $\mathbf{Y}(t)$  concatenates the subsequences of all dimensions into a one-dimensional vector.

$$\begin{aligned} \text{PE}_\alpha(P\|P') &\equiv PE(P\|\alpha P + (1-\alpha)P') \\ &= \frac{1}{2} \int p'_\alpha(\mathbf{X}) \cdot \left( \frac{p(\mathbf{X})}{p'_\alpha(\mathbf{X})} - 1 \right)^2 d\mathbf{X}, \end{aligned} \quad (2)$$

where  $p'_\alpha(\mathbf{X}) = \alpha p(\mathbf{X}) + (1-\alpha)p'(\mathbf{X})$  is the  $\alpha$ -mixture density. The  $\alpha$ -relative density-ratio is then defined as:

$$r_\alpha(\mathbf{X}) = \frac{p(\mathbf{X})}{p'_\alpha(\mathbf{X})} = \frac{p(\mathbf{X})}{\alpha p(\mathbf{X}) + (1-\alpha)p'(\mathbf{X})}, \quad (3)$$

which reduces to plain density-ratio when  $\alpha = 0$ , and it is bounded above by  $1/\alpha$  for  $\alpha > 0$ , even when the plain density-ratio  $\frac{p(\mathbf{X})}{p'(\mathbf{X})}$  is unbounded. The aim now is to estimate the quantity in (3) by a suitable model.

It is important to notice that neither (1) nor (2) are metrics, since they are not symmetric and the triangular inequality does not hold. To cope with the first problem, authors in Liu et al. (2013) proposed to use the symmetrical divergence:

$$\text{PE}_\alpha(P\|P') + \text{PE}_\alpha(P'\|P), \quad (4)$$

where each term is estimated separately. However, divergence (4) still not satisfies the triangle inequality: this issue will be postponed to future development.

### 2.3 Learning algorithm

The  $\alpha$ -relative density-ratio is modeled as:

$$g(\mathbf{X}; \boldsymbol{\theta}) \equiv \sum_{l=1}^n \theta_l \cdot K(\mathbf{X}, \mathbf{Y}_l), \quad (5)$$

where  $\boldsymbol{\theta} = [\theta_1, \dots, \theta_n]^T \in \mathbb{R}^{n \times 1}$  are unknown parameters,  $K(\cdot, \cdot)$  is a kernel basis function, and  $\mathbf{Y}_l$  refers to the  $l$ -th data sample in  $\mathcal{Y}(t)$ . In our experiments, we employ the Gaussian kernel such that:

$$K(\mathbf{Y}_1, \mathbf{Y}_2) = \exp\left(-\frac{\|\mathbf{Y}_1 - \mathbf{Y}_2\|^2}{2\delta^2}\right), \quad (6)$$

where  $\delta > 0$  is the kernel width. The parameters' vector  $\boldsymbol{\theta}$  is learned by minimizing the squared loss:

$$\begin{aligned} J(\boldsymbol{\theta}) &= \frac{1}{2} \int p'_\alpha(\mathbf{X}) \left( r_\alpha(\mathbf{X}) - g(\mathbf{X}; \boldsymbol{\theta}) \right)^2 d\mathbf{X} \\ &= \frac{1}{2} \int p'_\alpha(\mathbf{X}) r_\alpha^2(\mathbf{X}) d\mathbf{X} - \int p(\mathbf{X}) g(\mathbf{X}; \boldsymbol{\theta}) d\mathbf{X} \\ &\quad + \frac{\alpha}{2} \int p(\mathbf{X}) g(\mathbf{X}; \boldsymbol{\theta})^2 d\mathbf{X} + \frac{1-\alpha}{2} \int p'(\mathbf{X}) g(\mathbf{X}; \boldsymbol{\theta})^2 d\mathbf{X}, \end{aligned} \quad (7)$$

where the computations were made by expanding the square and employing the definition of  $p'_\alpha(\mathbf{X})$ .

The first term of (7) can be discarded since it does not depend on the unknown parameters. By substituting  $g(\mathbf{X}; \boldsymbol{\theta})$  with the definition (5), and approximating the expectations with empirical averages, it is possible to obtain the following minimization problem (with the addition of a Ridge regularization term  $\frac{\lambda}{2} \boldsymbol{\theta}^T \boldsymbol{\theta}$ ):

$$\hat{\boldsymbol{\theta}} = \arg \min_{\boldsymbol{\theta} \in \mathbb{R}^n} \left[ \frac{1}{2} \boldsymbol{\theta}^T \widehat{\mathbf{H}} \boldsymbol{\theta} - \widehat{\mathbf{h}}^T \boldsymbol{\theta} + \frac{\lambda}{2} \boldsymbol{\theta}^T \boldsymbol{\theta} \right], \quad (8)$$

where  $\widehat{\mathbf{H}} \in \mathbb{R}^{n \times n}$ ,  $\widehat{\mathbf{h}} \in \mathbb{R}^{n \times 1}$  and  $\lambda > 0$  controls the regularization strength.

The element in position  $(l, m)$  of  $\widehat{\mathbf{H}}$  is given by:

$$\begin{aligned} \widehat{H}_{(l,m)} &= \frac{\alpha}{n} \sum_{i=1}^n K(\mathbf{Y}_i, \mathbf{Y}_l) \cdot K(\mathbf{Y}_l, \mathbf{Y}_m) \\ &\quad + \frac{1-\alpha}{n} \sum_{j=1}^n K(\mathbf{Y}'_j, \mathbf{Y}_l) \cdot K(\mathbf{Y}'_j, \mathbf{Y}_m). \end{aligned} \quad (9)$$

The element in position  $l$  of  $\widehat{\mathbf{h}}$  is given by:

$$\widehat{h}_{(l)} = \frac{1}{n} \sum_{i=1}^n K(\mathbf{Y}_i, \mathbf{Y}_l). \quad (10)$$

The solution to problem (8) can expressed as:

$$\widehat{\boldsymbol{\theta}} = \left( \widehat{\mathbf{H}} + \lambda \mathbf{I}_n \right)^{-1} \cdot \widehat{\mathbf{h}}, \quad (11)$$

where  $\mathbf{I}_n$  is  $n$ -th dimensional identity matrix. The density ratio estimator assumes thus the form of:

$$\widehat{g}(\mathbf{X}) = \sum_{l=1}^n \widehat{\theta}_l \cdot K(\mathbf{X}, \mathbf{Y}_l). \quad (12)$$

### 2.4 Computing the divergence

In order to use (12), it is first necessary to rewrite the Pearson divergence (2) as:

$$\begin{aligned} \text{PE}_\alpha(P\|P') &= \frac{1}{2} \int p'_\alpha(\mathbf{X}) \cdot \left( \frac{p(\mathbf{X})}{p'_\alpha(\mathbf{X})} - 1 \right)^2 d\mathbf{X} \\ &= \frac{1}{2} \int p'_\alpha(\mathbf{X}) \cdot \left( \frac{p(\mathbf{X})^2}{p'_\alpha(\mathbf{X})^2} - 2 \frac{p(\mathbf{X})}{p'_\alpha(\mathbf{X})} + 1 \right) d\mathbf{X} \\ &= \frac{1}{2} \int \left( \frac{p(\mathbf{X})^2}{p'_\alpha(\mathbf{X})} - 2p(\mathbf{X}) + p'_\alpha(\mathbf{X}) \right) d\mathbf{X} \\ &= \frac{1}{2} \int \left( \frac{p(\mathbf{X})}{p'_\alpha(\mathbf{X})} \right) \cdot p(\mathbf{X}) d\mathbf{X} - \frac{1}{2}, \end{aligned} \quad (13)$$

where the simplification in the last step follows since probability distributions integrate to one. Replacing the estimator (12) in (13), and approximating the integrals with empirical averages, leads to the following approximation of the  $\alpha$ -relative divergence:

$$\widehat{\text{PE}}_\alpha = \frac{1}{2n} \sum_{i=1}^n \widehat{g}(\mathbf{Y}_i) - \frac{1}{2}. \quad (14)$$

The final computed score is then, as reported by (4), the quantity  $\Pi \equiv \widehat{\text{PE}}_\alpha(P\|P') + \widehat{\text{PE}}_\alpha(P'\|P)$ .

## 3. EXPERIMENTAL SETUP

The change detection methodology described in Section 2 has been applied to experimental data acquired from a test bench (see Figure 2), specifically suited to perform endurance tests on electro-mechanical actuators.

The considered EMA, used in aerospace environments, employs a three-phases brushless DC motor, with power supply redundancy. This makes the system capable to operate even in case of one supply loss. A Simplex LVDT with  $\pm 37$ mm of stroke is used for the position control loop. A ballscrew transmission, with 8 circuits with 1 turn each and 28 balls per turn, transforms the rotational motion in a linear one. The three phase currents are measured by LEM sensors. A linear motor provides the simulated load

that the EMA has to overcome. For a complete description of the experimental setup, see Mazzoleni et al. (2017b).

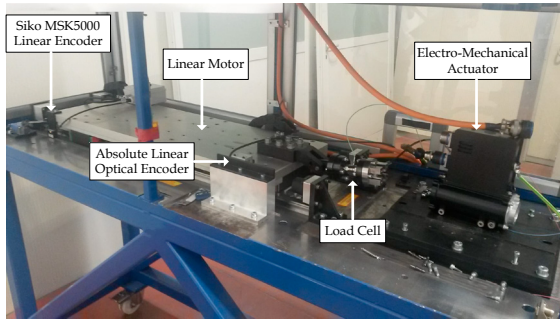


Fig. 2. Test bench with main components

In flight, the EMA has to actuate forward and backward the main flight control surfaces. For this reason, tests were done by imposing a sinusoidal position reference signal. The position control system of the EMA has been designed in such a way that the position tracking bandwidth is about 1.5Hz. Different amplitudes, ranging from 5mm to 30mm, and different frequencies, ranging from 0.1Hz to 10Hz, were used. The tests have been conceived to obtain a gradual deterioration of the specimen, in order to progressively acquire experimental data showing the process of degradation of the EMA until its complete failure. For this reason, we chosen to employ only 3 out of 8 balls circuits, to increase the pressure at the contact points between the balls and the screw thread. Furthermore, the EMA has been connected to the linear motor so that the 17% of the axial load force will generate also a radial component. In this way, an higher contact pressure will be obtained. The entity of the loads applied is obtained through a Finite Element Method (FEM) analysis, in order to understand in which conditions the balls are overstressed. The chosen load conditions are:

- **H0 condition:** 300N – nominal load condition
- **H1 condition:** 800N – overload condition
- **H1b condition:** 1200N – overload condition

The EMA suffered fatigue tests at conditions H1 and H1b. Measurements for the condition assessment were taken after every endurance session, in the H0 condition. Both overload conditions and the nominal one have been selected in each of the following different regimes:

- **Normal lubrication:** nominal operating condition
- **Poor lubrication:** lubricant *partially* removed
- **No lubrication:** lubricant *completely* removed

The choice of removing the lubricant from the mechanical transmission has been motivated by the fact that this is a possible fault that could occur in this types of actuators, and allowed the acceleration of EMA's wearing. Figure 3 reports the performed tests since April 2017. The term “cycles” refers to one period of the sinusoidal position profile. With the poor lubrication setting, the EMA performed a total of 76.640 cycles. In the no lubrication setting, the EMA performed a total of 135.600 cycles. Globally, the mechanical transmission performed 12.812.958 revolutions (this represents an overestimate since a proper consideration of the EMA dynamic response should be considered).

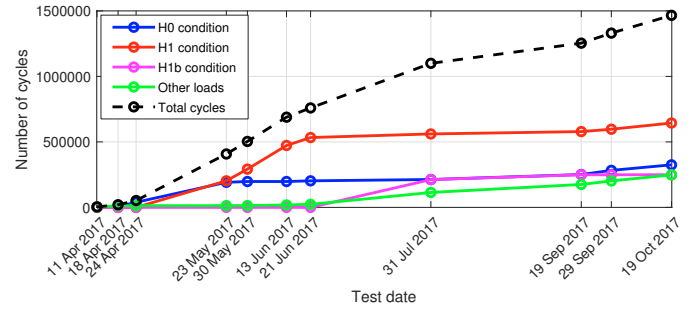


Fig. 3. Performed test conditions and number of cycles

## 4. CONDITION ASSESSMENT

### 4.1 Computation of the indicators

The condition assessment strategy that we employed is based on the assumption that mechanical components degradation will results in a loss of efficiency of the system. Thus, in order to obtain a correct position tracking, the EMA will drain more current. Because of this reasoning, different indicators were computed *only* on measured currents data, see Figure 4. Notice that, since the EMA is closed-loop controlled, until the power supply can provide enough energy, *we do not see any degradation* in position tracking. Monitoring the control actions, in this case the phase currents, helps into identifying possible causes of malfunction.

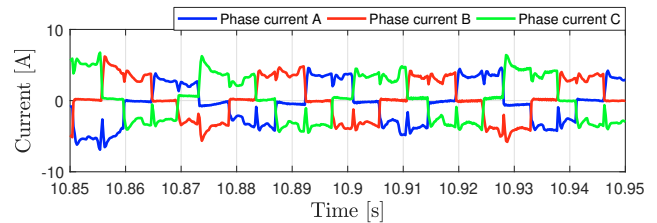


Fig. 4. Phase currents measured by LEM sensors

Consider now the three phase currents,  $i_a(t), i_b(t), i_c(t)$ , measured during an experiment. Since the measured position is a sinusoid with period  $T = 2\pi/\omega$ , with  $\omega$  the frequency measured in rad/s, it is possible to write the current signal of the  $x$ -th phase as:

$$i_x(t), \quad (\tau - 1) \cdot T \leq t \leq \tau \cdot T, \quad (15)$$

with  $x = a, b, c$  and  $\tau = 1, \dots, N_p$ , being  $N_p$  the total number of periods in the considered experiment. The aim now is to compute indicators on phase currents signals, in such a way that we can evaluate how they evolve in time. If the change detection algorithm detects that the *sampling distribution of the indicators* is changed, this is a symptom that the system is degraded in performance. In particular, two indicators have been computed from phase currents: the Root Mean Square (RMS) value and the Crest Factor (CF). The RMS is computed for each phase current  $x = a, b, c$  over a single period  $\tau = 1, \dots, N_p$  as follows:

$$\sigma_x(\tau) = \sqrt{\frac{1}{T} \cdot \sum_{t=(\tau-1) \cdot T}^{\tau \cdot T} i_x^2(t)}. \quad (16)$$

For each experiment, it is possible compute a mean RMS value at every period  $\tau = 1, \dots, N_p$  as:

$$\Sigma(\tau) = \frac{1}{3} \cdot (\sigma_a(\tau) + \sigma_b(\tau) + \sigma_c(\tau)) \in \mathbb{R} \quad (17)$$

The CF index is computed with the same rationale of the RMS value, and it is expressed as the ratio between the (absolute value of) the maximum peak of the signal and the RMS value, for  $x = a, b, c$  and  $\tau = 1, \dots, N_p$ :

$$\gamma_x(\tau) = \frac{\max(|i_x(t)|)}{\sigma_x(\tau)}, \quad (\tau - 1) \cdot T \leq t \leq \tau \cdot T. \quad (18)$$

For each experiment, it is possible compute a mean CF value at every period  $\tau = 1, \dots, N_p$  as:

$$\Gamma(\tau) = \frac{1}{3} \cdot (\gamma_a(\tau) + \gamma_b(\tau) + \gamma_c(\tau)) \in \mathbb{R} \quad (19)$$

The change-detection algorithm described in Section 3 will be applied to the features  $\Sigma(\tau)$  and  $\Gamma(\tau)$ . The former index has a clear physical meaning, it is expressed in Ampere; the latter is instead a pure number. The features  $\Sigma(\tau)$  and  $\Gamma(\tau)$  have been computed for a discrete range of operating frequencies. In particular, considered tests are those performed at frequencies of 0.1Hz, 0.3Hz, 0.5Hz, 0.8Hz, 0.9Hz and 1Hz. These range of frequencies is those for which the EMA has been designed. In the present work, we reported the application of the change-detection method to the chosen frequency of 1Hz. Notice that the proposed condition assessment scheme can be employed in an online manner, provided that the system will wait for the required samples before giving its response.

#### 4.2 Condition assessment as a change-detection problem

For the application of the proposed methodology, we consider a total of 11 experiments, performed at 1Hz with 10mm of position amplitude, in the H0 condition. The first 2 of these tests can be considered as *healthy state* experiments. Tests 3 and 4 have been performed after endurance sessions with *poor lubricant*. The remaining tests have been performed after endurance sessions with *no lubricant* at all. The experiments were then queued as if they were a unique time series.

The considered time series has dimensionality  $d = 2$ . Each sample  $\mathbf{y}(\tau) \in \mathbb{R}^{2 \times 1}$  is a vector which elements are  $\Sigma(\tau)$  and  $\Gamma(\tau)$ . Suppose for a moment that  $d = 1$ . Then, we would have that the RuLSIF method (see Figure 1), will compare a  $k$ -dimensional set of  $n$  data, contained in  $\mathcal{Y}(\tau)$ , with another similar set contained in  $\mathcal{Y}(\tau + n)$ . The parameter  $k$ , then, plays the role of a “memory” which usually appears in dynamic systems. Since we computed the value of the considered time series as independent indicators at each period  $\tau$ , we choose to set  $k = 1$ . Thus, we have that:

$$\mathbf{Y}(t) = \mathbf{y}(t) \in \mathbb{R}^{2 \times 1}. \quad (20)$$

The number of samples for each sliding window,  $n$ , is directly related to the convergence properties of the RuLSIF estimator, Kanamori et al. (2009). Here, however, we choose a more physical evaluation. In-fact,  $n$  is directly responsible for determining *how much detection delay* our condition assessment algorithm presents. With a small  $n$ , we can detect a distribution change faster, while being more sensible to data outliers and variations. Following discussions in Section 4, it is possible to find that the algorithm will have a “buffer zone” in the beginning, where

no response could be given, since it has to wait for all the needed data. This buffer has length  $\tau + 2n + k - 1$ . Since, at the start,  $\tau = 1$ , we have a buffer zone of  $1 + 2n + k - 1$  samples. It is straightforward to obtain an interpretation by knowing the period between every sample. In our experiment, each time series sample is issued every 1s, since we consider a sinusoidal reference position frequency of 1Hz. Considering a generic time  $\tau$ , the first datum of  $\mathcal{Y}(\tau)$  is issued at index  $\tau$ , while last appears at sample  $\tau + n + k - 2$ . The first datum of  $\mathcal{Y}(\tau + n)$  is issued at sample  $\tau + n$ , while the last at sample  $\tau + 2n + k - 2$ . Following these considerations, we chose to set  $n = 30$  samples, leading to a buffer zone of 59s and a change detection delay of 30s. The hyperparameters  $\delta$  and  $\lambda$  are chosen, for each couple of datasets  $\mathcal{Y}(\tau), \mathcal{Y}(\tau + n) \in \mathbb{R}^{2 \times 30}$  via  $\kappa$ -fold cross-validation. Since we follow the heuristic rule to have at least  $10 \cdot m$  data points, where  $m$  is the number of parameters to tune, it follows that we need at least 20 samples per fold. For this reason, we chose  $\kappa = 5$ . We then adhered to the default value  $\alpha = 0.5$  as in Liu et al. (2013).

The rationale for employing the RuLSIF method to perform a condition assessment task is as follows. First, we tuned a threshold value  $\eta$  based on the non-null scores  $\Pi(\tau)$  (since there is the buffer zone) returned from (14), from the first 2 experiments (those in healthy state). The threshold is tuned by taking the mean value  $\mu$  and standard deviation  $\nu$  of the aforementioned  $\Pi(\tau)$ , and setting  $\eta = \mu + 4 \cdot \nu$ . Then, the subsequent results returned by the algorithm were compared to  $\eta$ . If the obtained scores  $\Pi(\tau)$  are less than  $\eta$ , we set them to zero, otherwise we increment by one a “change-detection counter”  $\rho(\tau)$ . A decision can then be taken when  $\rho(\tau)$  exceeds a certain amount, depending on the specific application. Results are depicted in Figure 5. The first two plots depicts the computed indicators,  $\Gamma(\tau)$  and  $\Sigma(\tau)$ , respectively. The third plot depicts the score  $\Pi(\tau)$  (red), along with the computed threshold  $\eta$  (dot-dashed gray line) and the thresholded score (dotted black line). The last plot represents the change detection counter  $\rho(\tau)$ . The vertical dashed light gray lines represents the 11 different experiments used.

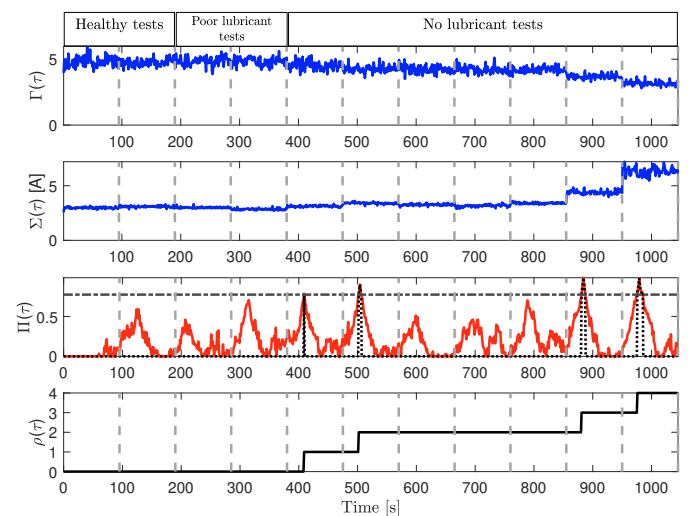


Fig. 5. Condition assessment via the RuLSIF method

Results in Figure 5 shows that, after 59s of buffer zone, the algorithm detects two significant changes from the

no lubricant tests. Afterwards, the distribution of the data does not change significantly until the last two experiments. Here it is possible to see from the value of the indicators that the mechanical transmission undergone a substantial damage, since the EMA requires high current values (the  $\Sigma(\tau)$  indicator) to perform the same task as before. It is interesting to notice that we were able to detect that a change in the EMA status occurred way before its final degraded behaviour.

## 5. CONCLUSIONS AND FUTURE DEVELOPMENTS

In this paper, we introduced a condition assessment algorithm for aerospace electro-mechanical actuators, by evaluating the distributional change of features computed from raw EMA measurements. The method, known in literature as RuLSIF, has been adapted in order to perform the health monitoring purposes. We tested the developed strategy on a set of experimental data measured during several months of endurance tests. Results show how the method is promising into identifying the distributional changes in the data, in an online manner. Future research is devoted to using metrics for comparing distributions (such as the Jensen-Shannon inequality), and an alternative tuning of the hyperparameters.

## ACKNOWLEDGEMENTS



This project has received funding from the the Clean Sky 2 Joint Undertaking under the European Union's Horizon 2020 research and innovation programme under grant agreement No 717112 (project acronym: REPRISE).

## REFERENCES

- Balaban, E., Saxena, A., Narasimhan, S., Roychoudhury, I., Koopmans, M., Ott, C., and Goebel, K. (2015). Prognostic health-management system development for electromechanical actuators. *Journal of Aerospace Information Systems*.
- Basseville, M., Nikiforov, I.V., et al. (1993). *Detection of abrupt changes: theory and application*, volume 104. Prentice Hall Englewood Cliffs.
- Buticchi, G., Costa, L., and Liserre, M. (2017). Improving system efficiency for the more electric aircraft: A look at dc/dc converters for the avionic onboard dc microgrid. *IEEE Industrial Electronics Magazine*, 11(3), 26–36.
- Byington, C.S., Watson, M., and Edwards, D. (2004). Data-driven neural network methodology to remaining life predictions for aircraft actuator components. In *Aerospace Conference, 2004. Proceedings. 2004 IEEE*, volume 6, 3581–3589. IEEE.
- Cognigni, A.L., Mazzoleni, M., and Previdi, F. (2016). Modeling and identification of an electro-hydraulic actuator. In *Control and Automation (ICCA), 2016 12th IEEE International Conference on*, 335–340. IEEE.
- Di Rito, G., Schettini, F., and Galatolo, R. (2017). Model-based health-monitoring of an electro-mechanical actuator for unmanned aerial system flight controls. In *Metrology for AeroSpace (MetroAeroSpace), 2017 IEEE International Workshop on*, 502–511. IEEE.
- Dixon, R. and Pike, A. (2002). Application of condition monitoring to an electromechanical actuator: a parameter estimation based approach. *Computing & Control Engineering Journal*, 13(2), 71–81.
- García, A., Cusido, I., Rosero, J., Ortega, J., and Romeral, L. (2008). Reliable electro-mechanical actuators in aircraft. *IEEE Aerospace and Electronic Systems Magazine*, 23(8).
- Garnett, R., Osborne, M.A., and Roberts, S.J. (2009). Sequential bayesian prediction in the presence of change-points. In *Proceedings of the 26th Annual International Conference on Machine Learning*, 345–352. ACM.
- Gibbs, A.L. and Su, F.E. (2002). On choosing and bounding probability metrics. *International statistical review*, 70(3), 419–435.
- Ismail, M.A., Balaban, E., and Spangenberg, H. (2016). Fault detection and classification for flight control electro-mechanical actuators. In *Aerospace Conference, 2016 IEEE*, 1–10. IEEE.
- Kanamori, T., Hido, S., and Sugiyama, M. (2009). A least-squares approach to direct importance estimation. *Journal of Machine Learning Research*, 10(Jul), 1391–1445.
- Kawahara, Y., Yairi, T., and Machida, K. (2007). Change-point detection in time-series data based on subspace identification. In *Data Mining, 2007. ICDM 2007. Seventh IEEE International Conference on*, 559–564. IEEE.
- Liu, S., Yamada, M., Collier, N., and Sugiyama, M. (2013). Change-point detection in time-series data by relative density-ratio estimation. *Neural Networks*, 43, 72–83.
- Mazzoleni, M., Maccarana, Y., and Previdi, F. (2017a). A comparison of data-driven fault detection methods with application to aerospace electro-mechanical actuators. *IFAC-PapersOnLine*, 50(1), 12797–12802. doi:10.1016/j.ifacol.2017.08.1837. 20th IFAC World Congress.
- Mazzoleni, M., Maccarana, Y., Previdi, F., Pispola, G., Nardi, M., Perni, F., and Toro, S. (2017b). Development of a reliable electro-mechanical actuator for primary control surfaces in small aircrafts. In *Advanced Intelligent Mechatronics (AIM), 2017 IEEE International Conference on*, 1142–1147. IEEE.
- Mazzoleni, M., Maroni, G., Maccarana, Y., Formentin, S., and Previdi, F. (2017c). Fault detection in airliner electro-mechanical actuators via hybrid particle filtering. *IFAC-PapersOnLine*, 50(1), 2860 – 2865. doi:10.1016/j.ifacol.2017.08.640. 20th IFAC World Congress.
- Pearson, K. (1992). On the criterion that a given system of deviations from the probable in the case of a correlated system of variables is such that it can be reasonably supposed to have arisen from random sampling. In *Breakthroughs in Statistics*, 11–28. Springer.
- Sarlioglu, B. and Morris, C.T. (2015). More electric aircraft: Review, challenges, and opportunities for commercial transport aircraft. *IEEE Transactions on Transportation Electrification*, 1(1), 54–64.
- Sugiyama, M., Suzuki, T., and Kanamori, T. (2012). *Density ratio estimation in machine learning*. Cambridge University Press.
- Yamanishi, K. and Takeuchi, J.i. (2002). A unifying framework for detecting outliers and change points from non-stationary time series data. In *Proceedings of the eighth ACM SIGKDD international conference on Knowledge discovery and data mining*, 676–681. ACM.
- Yeh, Y.C. (1996). Triple-triple redundant 777 primary flight computer. In *Aerospace Applications Conference, 1996. Proceedings., 1996 IEEE*, volume 1, 293–307. IEEE.